Mechanisms of Photostability in Kynurenines: A Joint Electronic-Structure and Dynamics Study

ARTICLE *in* THE JOURNAL OF PHYSICAL CHEMISTRY B · JULY 2014

Impact Factor: 3.3 · DOI: 10.1021/jp501782v · Source: PubMed

5 AUTHORS, INCLUDING:

Momir Mališ
Ruđer Bošković Institute
12 PUBLICATIONS **99** CITATIONS
SEE PROFILE

Andrzej L. Sobolewski
Polish Academy of Sciences
179 PUBLICATIONS **6,515** CITATIONS
SEE PROFILE

THE JOURNAL OF PHYSICAL CHEMISTRY B

Article

pubs.acs.org/JPCB

Mechanisms of Photostability in Kynurenines: A Joint Electronic-Structure and Dynamics Study

Deniz Tuna,*[,†,⊥] Nađa Došlić,[‡] Momir Mališ,[‡] Andrzej L. Sobolewski,[§] and Wolfgang Domcke[†]

[†]Department of Chemistry, Technische Universität München, 85747 Garching, Germany

[‡]Division of Physical Chemistry, Ruđer Bošković Institute, 10002 Zagreb, Croatia

[§]Institute of Physics, Polish Academy of Sciences, 02668 Warsaw, Poland

Supporting Information

ABSTRACT: Kynurenines are UV filters found in the human ocular lens which protect the retina from radiation damage. We report on *ab initio* investigations of the photochemistry of the *cis* and *trans* conformers of kynurenine and of an intramolecularly hydrogen-bonded conformer of 3-hydroxykynurenine *O*-*β*-D-glucoside. We have explored the excited-state reaction paths for several radiationless excited-state deactivation processes in kynurenines. We show that electron-driven proton-transfer processes mediated by an excited state of charge-transfer character exhibit negligible barriers and that the relevant potential-energy profiles are lower in energy than the lowest absorbing $\pi\pi^*$ state. In these proton-transfer processes, a proton moves from one of the amino groups of kynurenine to the keto group. We also report on nonadiabatic trajectory-surface-hopping molecular-dynamics simulations for photoexcited kynurenine. These simulations show that the *cis* and *trans* conformers of kynurenine deactivate on a femtosecond-to-picosecond time scale preferably via electron-driven proton transfer from one of the amino groups to the keto group. *Cis* kynurenine deactivates via a ring-N—H···O═C proton-transfer process. *Trans* kynurenine tends to undergo *trans* → *cis* isomerization before deactivating via the same process. These results suggest that the deactivation process involving the ring-amino group in the *cis* conformer of kynurenine is the most efficient excited-state deactivation process in kynurenines. The joint electronic-structure calculations and dynamics simulations provide a new level of mechanistic insight into the efficient UV-filtering capacity of kynurenines.

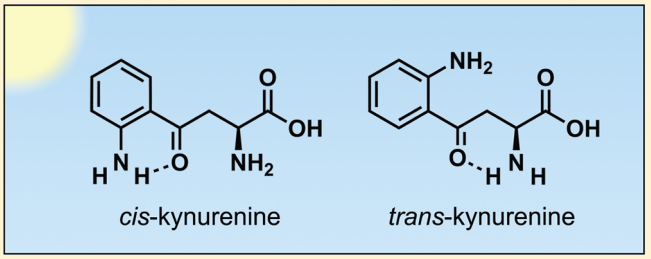

1. INTRODUCTION

Kynurenines are UV chromophores found in the human ocular lens.[1] They act as UV filters, thus protecting the retina from UV photodamage. While the cornea absorbs wavelengths below 300 nm, wavelengths from 300 to 400 nm (energies from 4.13 to 3.10 eV) are absorbed by several UV filters in the lens. Kynurenines found in the lens are metabolites of the amino acid tryptophan.[2] Figure 1 shows the structural formulas of kynurenines found in the human ocular lens. It is helpful to separate these six species into "small" species (the upper three species which carry hydroxyl, amino, and hydrogen rests) and "large" species (the lower three species which carry glucoside and glutathione rests). In the ocular lens, 3-hydroxykynurenine *O*-*β*-D-glucoside is found in the by far highest concentration of all kynurenines. Among the small kynurenines, kynurenine is found in the highest concentration.[3,4] These two species of kynurenines have been investigated in this work (cf. Figure 1).

Kynurenines have attracted the attention of researchers in photochemistry, photobiology, spectroscopy, ophthalmology, biochemistry, and organic chemistry. It has been shown that kynurenines possess an inherent chemical instability under physiological pH, which leads via deamination to the formation of an *α*,*β*-unsaturated ketone that can undergo Michael addition with nucleophilic side chains of proteins, such as lysine, cysteine, and histidine residues. This inherent chemical instability leads to the formation of adducts between kynurenines and proteins.[5] It has been found that the decrease in the concentration of kynurenines with age—which originates in their binding to amino acids and proteins[4,6,7]—as well as the generation of reactive oxygen species by these adducts[8,9] may be the cause for age-related cataract formation.[10,11]

Several spectroscopic studies have been performed on kynurenines as well as on derivatives and adducts of kynurenines in solution.[12−21] These studies include time-resolved measurements,[12,18−21] the determination of excited-state lifetimes[18−21] and of rate constants for various thermochemical and photochemical processes,[12−15,19,21] as well as the determination of the quantum yields for fluorescence,[12,13,18−21] for the formation of triplet states,[13,17−20] and for photofragmentation.[14,15,17,20,21] These experiments have shown that kynurenines generally exhibit a

Special Issue: Photoinduced Proton Transfer in Chemistry and Biology Symposium

Received: February 19, 2014
Revised: June 26, 2014

   dx.doi.org/10.1021/jp501782v | J. Phys. Chem. B XXXX, XXX, XXX−XXX

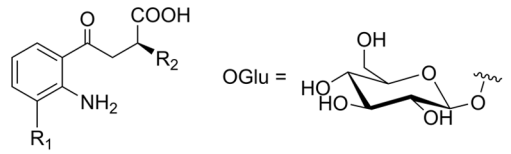

	R_1	R_2
kynurenine	H	NH_2
3-hydroxykynurenine	OH	NH_2
4-(2-aminophenyl)-4-oxobutanoic acid	H	H
3-hydroxykynurenine *O*-β-D-glucoside	OGlu	NH_2
4-(2-aminophenyl)-4-oxobutanoic acid *O*-β-D-glucoside	OGlu	H
gluthathionyl-kynurenine	H	GSH

Figure 1. Structural formulas of kynurenines found in the human ocular lens. The two species of kynurenines that have been investigated in this work are indicated in red. "GSH" stands for glutathione, a tripeptide formed from glutamic acid, glycine, and cysteine.

high UV photostability, a low propensity for generating photoproducts, a low propensity for populating excited triplet states, and a high propensity for thermal deamination. Vauthey, Sherin, and co-workers have shown that kynurenine in aqueous solution exhibits a quantum yield for internal conversion of about 98%, while the quantum yields for the population of triplet states and for fluorescence combined amount to less than 2%. They concluded that excited-state intramolecular as well as intermolecular proton transfer (solvent-assisted in the latter case) is responsible for the radiationless deactivation of electronically excited kynurenine.[18] The gas-phase absorption spectra of the isolated and protonated form of 3-hydroxykynurenine were measured by Kessel et al.[22] Kynurenine has also been used as a fluorescent probe for the investigation of protein dynamics (as an alternative to tryptophan).[23]

Only a few computational studies have been performed on kynurenines to date.[20,22,24] Kessel and co-workers compared the vertical excitation energies computed at the MCQDPT2 level of theory of neutral 3-hydroxykynurenine *in vacuo* and of neutral and zwitterionic forms of 3-hydroxykynurenine *in aquo* (treated by an effective fragment potential) and compared these values with the absorption spectra obtained in the gas phase and in the solution phase. They found that the absorption spectrum of 3-hydroxykynurenine undergoes a pronounced blue shift in going from the gas phase to aqueous solution.[22] Vauthey, Tsentalovich, and co-workers computed $S_0 \rightarrow S_1$ vertical excitation energies of kynurenine, 3-hydroxykynurenine, and 4-(2-aminophenyl)-4-oxobutanoic acid at the TDDFT level and analyzed the involved molecular orbitals.[20] Benassi and Sherin computed the vertical excitation energies and fluorescence emission energies of the zwitterionic form of kynurenine in various solvents employing a polarizable-continuum model and the semiempirical INDO/CIS method and found good agreement between the computed values and the previously obtained experimental spectra.[24]

It is an established fact that ultrafast photochemical reactions are mediated by critical points on the excited-state potential-energy surfaces, that is, conical intersections. These points are characterized by a diverging nonadiabatic coupling between the intersecting electronic states, which results in a complete breakdown of the Born−Oppenheimer approximation and an efficient conversion of electronic energy into vibrational energy. The exploration of the photochemical reaction path, that is, the mapping of the relevant excited-state potential-energy profiles from the Franck−Condon region to the relevant conical intersection, provides information on the kinetic significance of a photochemical reaction process. Kinetically accessible S_1/S_0 conical intersections can mediate efficient radiationless excited-state deactivation of photoexcited molecules via internal conversion to the electronic ground state and thus provide the mechanism for the high photostability of many organic molecules.[25−27]

Mixed quantum-classical molecular-dynamics simulations offer an efficient approach to treat the photoinduced molecular dynamics of medium-sized systems. In the trajectory-surface-hopping approach, the dynamics of the nuclei on the adiabatic potential-energy surfaces are treated classically by solving Newton's equations, while the electrons are treated quantum-mechanically according to the time-dependent Schrödinger equation. Nonadiabatic transitions between electronic states are taken into account by a stochastic algorithm. By simulating a large number of trajectories, the dynamics of a quantum-mechanical nuclear wavepacket can be approximated. Among the advantages of the trajectory-surface-hopping approach are the inclusion of all nuclear degrees of freedom in the dynamics simulations via on-the-fly computation of energy, gradients, and nonadiabatic couplings. This approach can provide valuable information on the time scales of radiationless excited-state deactivation processes and the statistical relevance of a particular process.[28−30]

Herein, we report on a systematic investigation of the photochemical mechanisms for radiationless excited-state deactivation of two conformers of kynurenine and one conformer of 3-hydroxykynurenine *O*-β-D-glucoside (cf. Figure 1 for the structural formulas). We performed explorations of the relevant excited-state potential-energy functions along various photochemical reaction paths and optimized the relevant conical intersections involved in the various deactivation processes. We have performed these explorations with the ADC(2) electronic-structure method. In addition to the static exploration of the excited-state potential-energy functions, we report the results of nonadiabatic trajectory-surface-hopping molecular-dynamics simulations of kynurenine. These dynamics simulations were performed with the TDDFT electronic-structure method, which is the method of choice for systems of this size.[31−33]

2. RESULTS

For kynurenine (cf. Figure 1), we considered the *cis* conformer, in which the central keto group is situated on the same side as the ring-amino group (cf. inset of Figure 3 for the structural formula), as well as the *trans* conformer, in which the central keto group is situated on the opposite side of the ring-amino group (cf. inset of Figure 5 for the structural formula). For these two conformers of kynurenine, we explored the relevant singlet excited-state potential-energy functions along various photochemical reaction paths for radiationless excited-state deactivation. We also performed nonadiabatic on-the-fly molecular-dynamics simulations employing the trajectory-surface-hopping method.

2.1. Electron-Driven Proton Transfer in the Ring-N—H···O=C Intramolecularly Hydrogen-Bonded *cis* Conformer of Kynurenine. Figure 2a shows the ground-state equilibrium geometry of the ring-N—H···O=C

dx.doi.org/10.1021/jp501782v | J. Phys. Chem. B XXXX, XXX, XXX−XXX

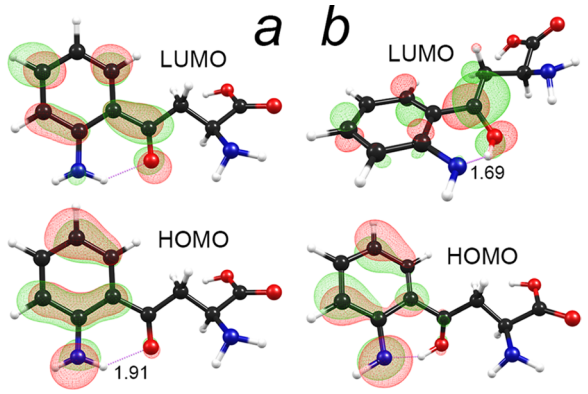

Figure 2. Optimized geometries and frontier orbitals of the intramolecularly hydrogen-bonded *cis* conformer of kynurenine: (a) molecular structure and orbitals of the ground-state equilibrium geometry; (b) molecular structure and orbitals of the S_1/S_0 conical intersection. Shown are the highest-occupied π orbital and the lowest-unoccupied π^* orbital of the lowest-lying $\pi\pi^*$ state of charge-transfer character, which mediates an electron-driven proton-transfer process. The length of the relevant hydrogen bond is indicated (in Å). For details, consult the Computational Methods section.

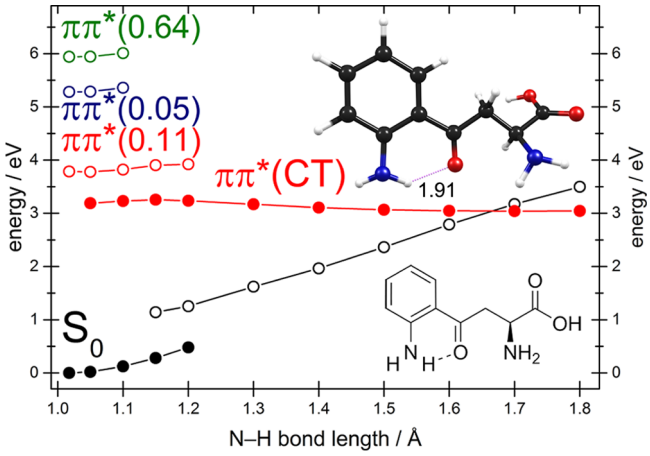

Figure 3. Energy profiles (in eV) of the electronic ground state (S_0) and three optically bright $\pi\pi^*$ states for the intramolecularly hydrogen-bonded *cis* conformer of kynurenine. The energy profiles were obtained by a constrained relaxed scan along the ring-N–H internuclear distance in the electronic ground state (full black circles) and in the first $\pi\pi^*$ state (full red circles). The vertical excitation energies of the $\pi\pi^*$ states (empty red, blue, and green circles) and the vertical energies of the ground state (empty black circles, see text) are also given. The values of the oscillator strengths at the ground-state equilibrium geometry are given in parentheses. The insets show the structural formula of the intramolecularly hydrogen-bonded *cis* conformer and the ground-state equilibrium geometry with the length of the intramolecular hydrogen bond (in Å). The energy profiles of the $n\pi^*$ states are not shown for clarity. For details, consult the Computational Methods section.

intramolecularly hydrogen-bonded *cis* conformer and the two frontier orbitals of the lowest-lying $\pi\pi^*$ state of kynurenine (cf. Computational Methods). The lowest $\pi\pi^*$ state is primarily a HOMO → LUMO transition, which involves a significant translocation of electron density from the ring-amino group to the keto group of the molecule, resulting in a pronounced charge-transfer character of this state. Figure 2b shows the optimized geometry of the S_1/S_0 conical intersection (cf. Computational Methods) involved in the radiationless excited-state deactivation process via the electron-driven proton transfer between the ring-amino group and the keto group (v.i.). The charge-transfer character of the $\pi\pi^*$ state is even more evident at the geometry of the conical intersection than at the ground-state equilibrium geometry, since the LUMO is located primarily on the keto group and only to a minor degree on the aniline moiety (cf. Figure 2b).

Figure 3 shows the potential-energy profiles (cf. Computational Methods) of the electronic ground state and of three optically bright $\pi\pi^*$ states along the proton-transfer reaction path. The driving coordinate is the N–H bond length of the ring-amino group. It describes the movement of a proton from the ring-amino group to the oxygen atom of the keto group. The full black circles represent the potential-energy profile of the electronic ground state along the reaction path optimized in the electronic ground state. The vertical excitation energies of three $\pi\pi^*$ states along this reaction path are given by the empty red, blue, and green circles. The numbers in parentheses specify the oscillator strengths of the excited states at the ground-state equilibrium geometry (structure shown as an inset in Figure 3). While the first two $\pi\pi^*$ states are moderately bright, the third $\pi\pi^*$ state is strongly absorbing. The full red circles in Figure 3 represent the potential-energy profile of the charge-transfer state along the reaction path optimized in this state. The energy of the ground state at the same geometries is given by the empty black circles. The potential-energy profile of the $\pi\pi^*$(CT) state exhibits a very low barrier for proton transfer from the amino to the keto group. This tiny barrier should not affect the kinetics of the proton-transfer process, since the potential-energy function for the optimized geometries of the first $\pi\pi^*$ state is located well below the vertical excitation energy of this state at the ground-state equilibrium geometry. The pronounced charge-transfer character of the lowest-lying singlet excited $\pi\pi^*$ state in the intramolecularly hydrogen-bonded *cis* conformer of kynurenine drives the transfer of a proton from the ring-amino group to the keto group. The movement of the proton from the ring-amino group to the keto group has an opposed effect on the energies of the charge-transfer state and the electronic ground state: while the energy of the charge-transfer state drops, the energy of the ground state rises. The potential-energy profiles of the charge-transfer state and the electronic ground state intersect at an N–H distance of ~1.7 Å, which gives rise to a conical intersection. The optimized geometry of this conical intersection is shown in Figure 2b. This conical intersection provides the photochemical funnel for ultrafast internal conversion to the electronic ground state. After the system has deactivated to the ground state, the slope in the potential-energy profile of the ground state toward shorter N–H distances drives the proton back to the ring-amino group. Thus, the ultrafast forward–backward transfer of a proton (v.i.) converts electronic energy into vibrational energy of the electronic ground state before deleterious photochemical reactions can proceed.

2.2. Electron-Driven Proton Transfer in the Tail-N—H···O═C Intramolecularly Hydrogen-Bonded *trans* Conformer of Kynurenine. Figure 4a shows the ground-state equilibrium geometry of the tail-N—H···O═C intramolecularly hydrogen-bonded *trans* conformer and the two singly occupied molecular orbitals of the principal configuration of the lowest excited singlet state. The lowest excited singlet state of this conformer is an $n\pi^*$ state, which originates from the excitation of an electron from the lone-pair orbital of the oxygen atom of the keto group to a π^* orbital on the

dx.doi.org/10.1021/jp501782v | J. Phys. Chem. B XXXX, XXX, XXX–XXX

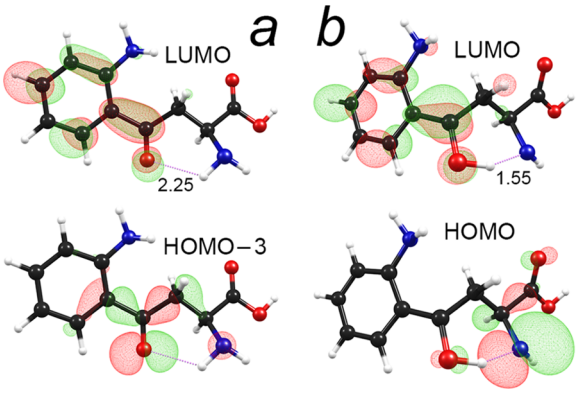

Figure 4. Optimized geometries and molecular orbitals of the intramolecularly hydrogen-bonded *trans* conformer of kynurenine: (a) molecular structure and orbitals of the ground-state equilibrium geometry; (b) molecular structure and orbitals of the S_1/S_0 conical intersection. Shown are the singly occupied molecular orbitals of the lowest excited singlet state at the respective molecular structures. The length of the relevant hydrogen bonds is indicated (in Å). For details, consult the Computational Methods section.

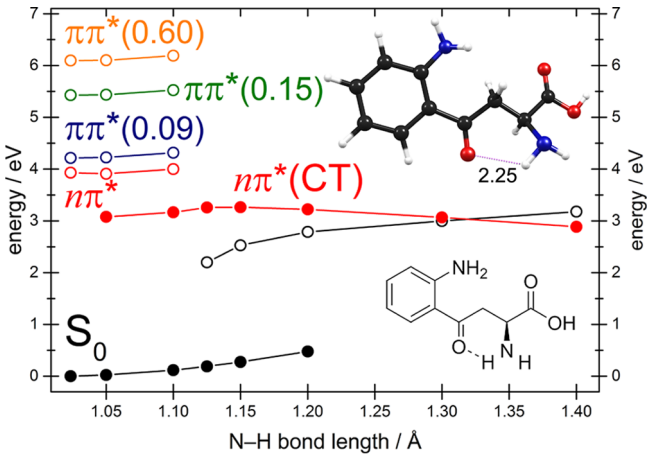

Figure 5. Energy profiles (in eV) of the electronic ground state (S_0), the lowest $n\pi^*$ state, and three optically bright $\pi\pi^*$ states for the intramolecularly hydrogen-bonded *trans* conformer of kynurenine. The energy profiles were obtained by a constrained relaxed scan along the tail-N−H internuclear distance in the electronic ground state (full black circles) and in the $n\pi^*$(CT) state (full red circles). The vertical excitation energies of the lowest $n\pi^*$ (empty red circles) and the three $\pi\pi^*$ states (empty blue, green, and orange circles) and the vertical energies of the ground state (empty black circles) are also given. The values of the oscillator strengths at the ground-state equilibrium geometry are given in parentheses. The insets show the structural formula of the intramolecularly hydrogen-bonded *trans* conformer and the ground-state equilibrium geometry with the length of the intramolecular hydrogen bond (in Å). For details, consult the Computational Methods section.

acetophenone moiety. The extension of the π system over the keto group is noteworthy. Figure 4b shows the optimized geometry of the S_1/S_0 conical intersection involved in the radiationless excited-state deactivation process via electron-driven proton transfer between the tail-amino group and the keto group (v.i.). The $S_1(n\pi^*)$ state at the conical intersection originates from the excitation of an electron from the lone-pair orbital of the nitrogen atom of the tail-amino group to a π^* orbital of the acetophenone moiety. While at the ground-state equilibrium geometry the S_1 state is a locally excited $n\pi^*$ state, it exhibits a charge-transfer character from the tail-amino group to the keto group at the optimized geometry of the conical intersection. The locally excited character of the $n\pi^*$ state at the former and the charge-transfer character at the latter structure are also evident from the dipole moment of the S_1 state at these geometries: 3.7 D at the ground-state equilibrium geometry and 6.2 D at the optimized geometry of the conical intersection (for comparison, the dipole moment of the electronic ground state at the ground-state equilibrium geometry is 1.6 D).

Figure 5 shows the potential-energy profiles of the electronic ground state, of the lowest $n\pi^*$ state, and of three bright $\pi\pi^*$ states along the proton-transfer reaction path. The driving coordinate is the N−H bond length of the tail-amino group. It describes the movement of a proton from the tail-amino group to the oxygen atom of the keto group. The full black circles represent the potential-energy profile of the electronic ground state along the reaction path optimized in the electronic ground state. The vertical excitation energies of the $n\pi^*$ state and of the three bright $\pi\pi^*$ states are given by the empty red, blue, green, and orange circles. The numbers in parentheses specify the oscillator strengths of the excited states at the ground-state equilibrium geometry (structure shown as an inset in Figure 5). While the first two $\pi\pi^*$ states are moderately bright, the third $\pi\pi^*$ state is strongly absorbing. The full red circles in Figure 5 represent the potential-energy profile of the $n\pi^*$(CT) state along the reaction path optimized in this state. The energy of the ground state at the same geometries is given by the empty black circles. The character of the $S_1(n\pi^*)$ state changes from a locally excited state to a charge-transfer state with increasing N−H distance. Thus, electron density moves from the tail-amino group to the keto group. The potential-energy function of the first excited singlet state exhibits a very low barrier. This minor barrier should not affect the kinetics of the proton-transfer process, since the potential-energy function of the first excited singlet state is located well below the vertical excitation energy of the lowest $\pi\pi^*$ state at the ground-state equilibrium geometry. The charge-transfer character of the $S_1(n\pi^*)$ state in the intramolecularly hydrogen-bonded *trans* conformer of kynurenine drives the transfer of a proton from the tail-amino group to the keto group. The potential-energy profiles of the charge-transfer state and the electronic ground state intersect at an N−H distance of ~1.3 Å, which gives rise to a conical intersection. The optimized geometry of this conical intersection is shown in Figure 4b. In contrast to subsection 2.1, the N−H bond length of the conical intersection indicated by the potential-energy profiles (~1.3 Å) varies significantly from the value found in the optimized structure of the conical intersection (1.55 Å) for this conformer. The geometry optimization was performed without any constraints (cf. Computational Methods), allowing a slight conformational change in the tail of the molecule, which leads to a longer N−O distance (by ~0.2 Å) and, thus, to a longer N−H distance in the conical intersection of the *cis* conformer. The conical intersection provides the photochemical funnel for ultrafast internal conversion to the ground state. After the system has deactivated to the ground state, the slope of the potential-energy profile of the ground state toward shorter N−H distances drives the proton back to the tail-amino group, albeit the slope of the ground state appears to be much gentler than that for the *cis* conformer (cf. Figure 3).

2.3. Ring-Puckering Deactivation Mechanisms in Kynurenine. We have also considered deactivation mechanisms which are inherent to the phenyl moiety. While these

dx.doi.org/10.1021/jp501782v | J. Phys. Chem. B XXXX, XXX, XXX−XXX

mechanisms apply to all conformers, we have chosen the *trans* conformer of kynurenine for the exploration of the energy profiles of these mechanisms. Benzene is known to exhibit radiationless deactivation of the S_1 state via a ring-puckering mechanism, which is also known as the "channel-3 pathway".[34−36] Analogous deactivation processes have been identified in aniline.[37] For the characterization of these ring-puckering deactivation processes in kynurenine, we have optimized three conical intersections which exhibit an out-of-plane geometry for one of the carbon atoms of the aniline moiety. Two of the three optimized conical intersections exhibit an out-of-plane geometry in the carbon atoms in α-position to the amino group. In one of these intersections, the amino group is displaced above the plane of the benzene ring, and in the other, it is displaced below the plane. We selected one of these optimized conical intersections and constructed a linearly interpolated reaction path between it and the ground-state equilibrium geometry. The energy profiles of the electronic ground state and the three lowest $\pi\pi^*$ states along this linearly interpolated reaction path are shown in Figure 6.

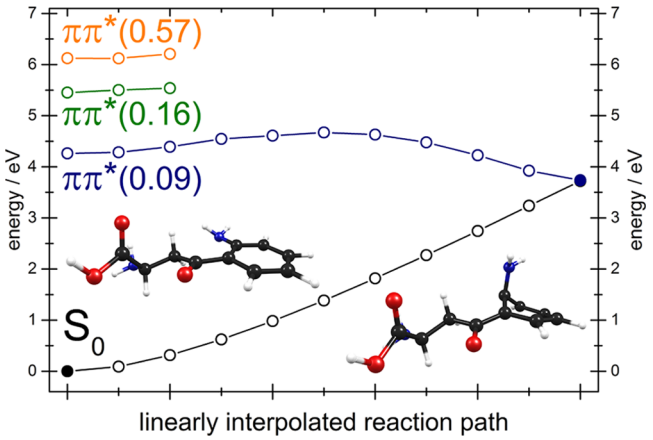

Figure 6. Energy profiles (in eV) of the electronic ground state (empty black circles) and three optically bright $\pi\pi^*$ states (empty blue, green, and orange circles) along the linearly interpolated reaction path from the ground-state equilibrium geometry (full black circle at the left bottom) to the ring-puckered conical intersection (full blue and black circles at the right). The values of the oscillator strengths at the ground-state equilibrium geometry are given in parentheses. For clarity, the energy profile of the $S_1(n\pi^*)$ state is not shown. The insets show the ground-state equilibrium geometry (left) and the geometry of the ring-puckered conical intersection (right). For details, consult the Computational Methods section.

The energy profile of the lowest $\pi\pi^*$ state exhibits an apparent barrier of around 0.6 eV, as found for the analogous reaction path in benzene and in aniline.[34−37] The true barrier is lower and likely is similar to benzene and aniline (3000 cm^{-1} (0.37 eV) in benzene). The optimized geometries of the remaining two ring-puckered conical intersections of kynurenine are shown in Figure S1 in the Supporting Information. The $\pi\pi^*$ state at the conical intersections involves π and π^* orbitals which are located exclusively on the phenyl moiety. The existence of several ring-puckered conical intersections involving an out-of-plane displacement of various atoms reflects the floppiness of the aromatic ring after $\pi \rightarrow \pi^*$ excitation. The ring-puckered conical intersections are located above 3.5 eV, while the proton-transfer conical intersections are located at ~3.0 eV.

2.4. Ring-Amino-Twist Deactivation Mechanism in Kynurenine. Apart from deactivation mechanisms which are mediated by excited-state proton transfer or by ring-puckering of the phenyl moiety, we have also identified a mechanism which is mediated by the twist motion of the ring-amino group. We have optimized a conical intersection which exhibits a perpendicular orientation of the ring-amino group with respect to the phenyl moiety. Figure 7 shows the energy profiles of the relevant electronic states along the linearly interpolated reaction path for the ring-amino-twist mechanism. The reaction path was constructed between the ground-state equilibrium geometry of the *cis* conformer of kynurenine and the S_1/S_0 conical intersection. After excitation to the lowest $\pi\pi^*$ state, the system can undergo internal conversion to the $n\pi^*$ state. The reaction path from the reactive $n\pi^*$ state to the conical intersection with the ground state is completely barrierless. We have also located an excited-state equilibrium geometry on the $n\pi^*$ potential-energy surface, which is located between the last two points of the linearly interpolated reaction path shown in Figure 7 (indicated by an arrow). This suggests that this S_1 minimum is very close to the conical intersection, the only difference between this minimum and the conical intersection being a slight deviation in the C═O bond length of the keto group. Therefore, the presented reaction path reveals another presumably efficient mechanism for radiationless excited-state deactivation of kynurenine. The energy of the amino-twist conical intersection is 3.0 eV, which is the same as the energies of the proton-transfer conical intersections.

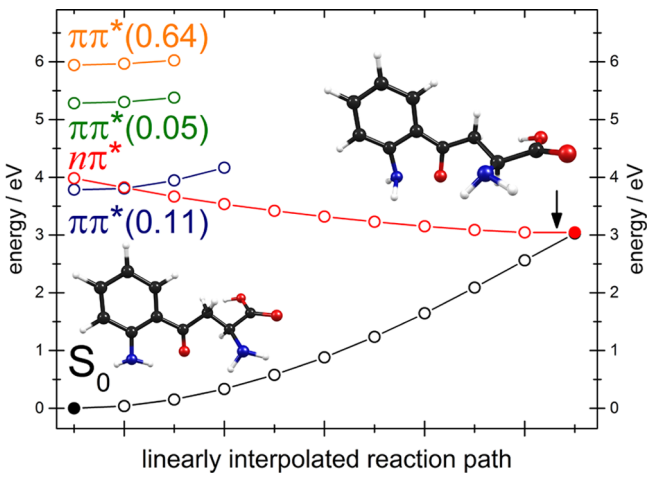

Figure 7. Energy profiles (in eV) of the electronic ground state (empty black circles), the lowest $n\pi^*$ state (empty red circles), and three optically bright $\pi\pi^*$ states (empty blue, green, and orange circles) along the linearly interpolated reaction path from the ground-state equilibrium geometry (full black circle at the left bottom) to the amino-twisted conical intersection (full red and black circles at the right). The values of the oscillator strengths at the ground-state equilibrium geometry are given in parentheses. The insets show the ground-state equilibrium geometry (left) and the geometry of the amino-twisted conical intersection (right). The arrow indicates the location of the $n\pi^*$ excited-state equilibrium geometry along the interpolated path. For details, consult the Computational Methods section.

2.5. Nonadiabatic Trajectory-Surface-Hopping Molecular-Dynamics Simulations for Kynurenine. In this subsection, we present nonadiabatic trajectory-surface-hopping molecular-dynamics simulations for kynurenine using the

dx.doi.org/10.1021/jp501782v | J. Phys. Chem. B XXXX, XXX, XXX−XXX

TDDFT method with the B3LYP functional. Hybrid quantum-mechanical/classical nonadiabatic trajectory-surface-hopping dynamics simulations require the calculation of ensembles of trajectories to obtain information on the photochemical reactivity of the system. We have performed these simulations for a total duration of 1.5 ps for a batch of trajectories initiated in the S_1 state for both the *cis* and *trans* conformers of kynurenine. We aimed at unraveling the time scales and the statistical relevance of the mechanisms presented in subsections 2.1−2.4. (For details of the simulation protocols, consult the Computational Methods section.)

Figure 8 shows the average population of the S_1 state during the dynamics simulations as well as an exponential fit for the

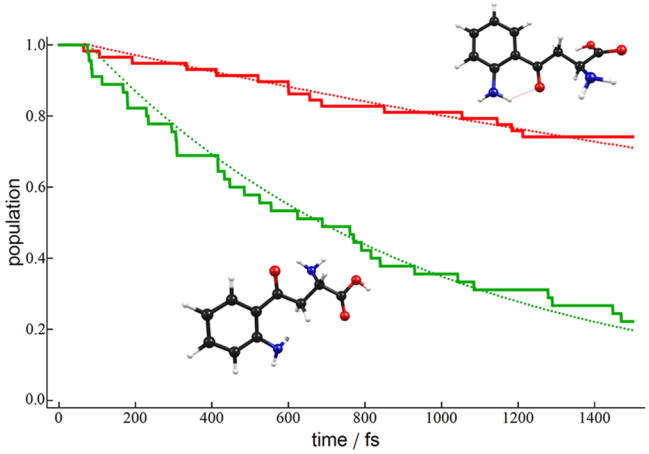

Figure 8. Average population of the first excited electronic state (S_1) obtained with nonadiabatic dynamics simulations for *cis* kynurenine (red) and *trans* kynurenine (green). The dotted lines represent exponential fits for the population probability of the S_1 state. They correspond to effective S_1 lifetimes of 4.1 ps (*cis* conformer) and 0.96 ps (*trans* conformer). The insets show representative molecular structures of the *cis* conformer (right top) and of the *trans* conformer (bottom).

determination of the lifetime of the S_1 state. The lifetime of the two conformers has been obtained by fitting the population probability of the S_1 state to a monoexponential decay function, $y = e^{-(t-t_1)/t_2}$, where t_1 is the initial delay time (the time needed for the first trajectory to reach the S_1/S_0 conical-intersection seam), t_2 is a decay constant, and $\tau = t_1 + t_2$ is the lifetime.[38] It is evident that the deactivation of *cis* kynurenine is less efficient than the deactivation of *trans* kynurenine. A major part of the trajectories of *cis* kynurenine remains in the S_1 state, resulting in an effective lifetime of 4.1 ps, while the S_1 lifetime of the *trans* conformer is only 0.96 ps.

Table 1 gives the statistical distribution of the various deactivation mechanisms found for the trajectories initiated in the S_1 state of the *cis* and *trans* conformers of kynurenine. After 1.5 ps of simulation time, 36% of the trajectories of *cis* kynurenine and 74% of the trajectories of *trans* kynurenine have deactivated to the electronic ground state. As expected from the reaction-path studies, the dominant excited-state deactivation mechanism observed in the nonadiabatic dynamics simulations for kynurenine is electron-driven proton transfer. In merely four trajectories, we observed C−H bond fission after deactivation to the electronic ground state. In four other trajectories, various geometrical distortions of the molecule (other than the clearly recognizable proton-transfer process) raised the energy of the ground state to such an extent that an $S_1 \rightarrow S_0$ surface hop occurred. In *cis* kynurenine, proton transfer from the ring-amino group to the keto group accounts for 71% of the deactivated trajectories, while the remaining trajectories deactivated via proton transfer from the tail-amino group to the keto group. In *trans* kynurenine, on the other hand, proton transfer from the ring-amino group to the carbonyl oxygen atom of the acid group has been observed in more trajectories than proton transfer from the tail-amino group to the keto group.

Figure 9 shows the populated states and their instantaneous energies for a characteristic nonadiabatic trajectory for the *cis* conformer of kynurenine. The trajectory was initiated in the $S_1(\pi\pi^*)$ state (cf. red dots in Figure 9). This state exhibits charge-transfer character involving translocation of electron density from the ring-amino group to the keto group (cf. Figure 2). This translocation of electron density induces the transfer of a proton from the ring-amino group to the keto group. The spike in the energy of the electronic ground state at about 50 fs is due to a planarization of the ring-amino group. The first attempt of proton transfer occurs at about 250 fs and involves a displacement of the oxygen atom out of the plane of the six-membered ring formed by the intramolecular hydrogen bond. This results in a destabilization of the ground state (black curve) by ∼1.8 eV. After 590 fs, the proton transfer from the ring-amino group to the keto group occurs due to the vanishing S_1/S_0 energy gap and the resulting strong nonadiabatic coupling between these two states. The subsequent propagation on the ground-state potential-energy surface involves a back-transfer of the proton to the ring-amino group and redistribution of the excess vibrational energy from the initially excited ring-N−H stretching vibration (which causes the high-frequency large-amplitude fluctuations of the potential-energy profiles) to lower-frequency vibrations involving the keto group at about 0.8 ps. The Fourier analysis of the time-dependent potential energy of the ground state between 600 and 975 fs, which reveals the contributions of various vibrational normal modes in the vibrational-energy-redistribution process, is presented in Figure S2 in the Supporting Information.

Table 1. Statistical Distribution of Excited-State Deactivation Processes for All Simulated Trajectories of the *cis* and *trans* Conformers of Kynurenine

conformer	N^a	$N_{S_0}{}^b$	ring-N—H···O=C^c	tail-N—H···O=C^d	ring-N—H···O=COH^e	other^f
cis	58	21	15	5	0	1
trans	50	37	15	6	9	7

[a]Total number of simulated trajectories. [b]Number of simulated trajectories that have deactivated to the S_0 within 1.5 ps. [c]Number of simulated trajectories that have deactivated to the S_0 via ring-N—H···O=C proton transfer. [d]Number of simulated trajectories that have deactivated to the S_0 via tail-N—H···O=C proton transfer. [e]Number of simulated trajectories that have deactivated to the S_0 via ring-N—H···O=COH proton transfer. [f]Number of simulated trajectories that have deactivated to the S_0 via a different mechanism.

dx.doi.org/10.1021/jp501782v | J. Phys. Chem. B XXXX, XXX, XXX−XXX

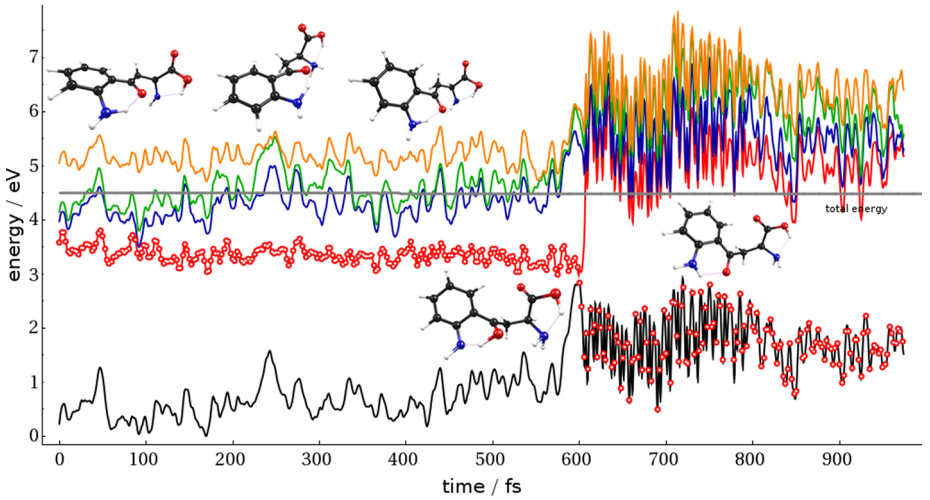

Figure 9. Instantaneous energies of the electronic ground state (S_0, black curve) and the first four excited singlet states (S_1–S_4, red, blue, green, and orange curves) for a selected trajectory of *cis* kynurenine, obtained with nonadiabatic trajectory-surface-hopping dynamics simulations. The red dots indicate the populated state at a given time. At 600 fs, the trajectory hops to the S_0 state at the S_1/S_0 conical intersection. The insets show selected molecular structures during the time evolution of the trajectory. The value of the total energy of the system is given by the horizontal line. For details, consult the Computational Methods section.

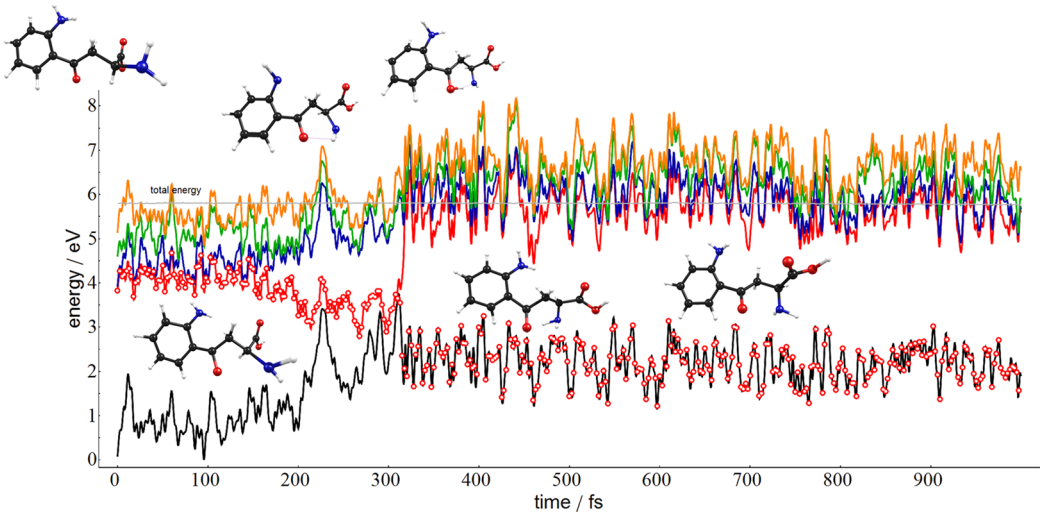

Figure 10. Instantaneous energies of the electronic ground state (S_0, black curve) and the first four excited singlet states (S_1–S_4, red, blue, green, and orange curves) for a selected trajectory of *trans* kynurenine, obtained by nonadiabatic trajectory-surface-hopping dynamics simulations. The red dots indicate the populated state at a given time. At 300 fs, the trajectory hops to the S_0 state at the S_1/S_0 conical intersection. The insets show selected molecular structures during the time evolution of the trajectory. The value of the total energy of the system is given by the horizontal line. For details, consult the Computational Methods section.

Figure 10 shows the populated states and their instantaneous energies for a selected nonadiabatic trajectory of *trans* kynurenine deactivating via proton transfer from the tail-amino group to the keto group. During the first 200 fs of the dynamics, the system propagates on the S_1 surface. Since the energy gap between the S_1 and S_2 surfaces is small (<0.1 eV), the two states exhibit both $\pi\pi^*$ and $n\pi^*$ character. In the $n\pi^*$ configuration, electron density is shifted from the lone-pair orbital of the oxygen atom of the keto group to the aniline ring (cf. Figure 4a). The rotation of the tail of the molecule, noticeable by the increase of the energy of the electronic ground state after ∼200 fs, is initiated by the change of character of the S_1 state. From 160 fs onward, the S_1 state acquires some $n\pi^*$ character with an increasing contribution from the lone-pair orbital of the nitrogen atom of the tail-amino group (as has been discussed in subsection 2.2 and shown in Figure 4b). Once the weight of this contribution dominates the wave function of this excited state at ∼300 fs, a proton transfer from the tail-amino group to the keto group takes place. The subsequent propagation on the ground-state potential-energy surface reveals a rotation of the tail-amino group.

As stated above, the two dominating deactivation mechanisms observed in the trajectories of *cis* kynurenine are proton transfer from the ring-amino group to the keto group and proton transfer from the tail-amino group to the keto group (cf. Table 1). It is interesting to note the complete absence of the ring-amino-twist deactivation mechanism. While ring-amino-twisted structures have been frequently spotted during the dynamics simulations and led to a reduction of the S_1/S_0 energy gap to only 0.4–0.3 eV, a subsequent deactivation to the ground state has never been observed. From Figure 7, it is apparent that, at the geometry of the ring-amino-twist

dx.doi.org/10.1021/jp501782v | J. Phys. Chem. B XXXX, XXX, XXX–XXX

minimum on the $S_1(n\pi^*)$ surface, the S_1/S_0 energy gap is smaller than 0.5 eV at the ADC(2) level. At the TDDFT level, on the other hand, the corresponding S_1/S_0 energy gap is 1.47 eV (see Figure S3 in the Supporting Information). This suggests that TDDFT provides an erroneous description of the potential-energy surface in the vicinity of the amino-twisted minimum and that the slower deactivation of the *cis* conformer compared to the *trans* conformer can be attributed in part to the inadequacy of the TDDFT method in correctly describing this part of the potential-energy surface.

In *trans* kynurenine, proton transfer from the ring-amino group to the carbonyl oxygen atom of the acid group has been observed, which constitutes a mechanism that we had not considered in the reaction-path explorations. This mechanism requires a *trans* → *cis* isomerization of kynurenine prior to the formation of an intramolecular ring-N—H···O═C hydrogen bond and ensuing proton transfer along this hydrogen bond. The absorbing state is the lowest $\pi\pi^*$ state in *trans* kynurenine, which is energetically close to the lowest $n\pi^*$ state (cf. Figure 5). The translocation of electron density from the aniline ring to the keto group in the $\pi\pi^*$ state weakens the C—C bond connecting the two groups and facilitates isomerization. Two additional trajectories of *trans* kynurenine undergoing *trans* → *cis* isomerization followed by excited-state deactivation via ring-N—H···O═C proton transfer and ring-N—H···O═COH proton transfer, respectively, are shown in Figures S4 and S5 in the Supporting Information. In *trans* kynurenine, proton transfer from the ring-amino or tail-amino groups to the keto group accounts for 57% of the deactivated trajectories, while, in 24% of the trajectories, proton transfer from the ring-amino group to the carbonyl oxygen of the carboxyl group takes place.

We did not observe any trajectories deactivating via one of the ring-puckering processes discussed in subsection 2.3. This suggests that the barrier on the reaction path of the ring-puckering processes is too high and the effective nuclear mass too large for competition with the electron-driven proton-transfer processes, which involve negligible barriers and the movement of the light hydrogen atom.

2.6. Electron-Driven Proton Transfer in 6′-O—H···N2 Intramolecularly Hydrogen-Bonded Conformers of 3-Hydroxykynurenine *O*-β-D-Glucoside. It is a reasonable assumption that all mechanisms found for kynurenine should be available in 3-hydroxykynurenine *O*-β-D-glucoside as well. We contemplated which types of photochemical deactivation mechanisms, aside from the ones we have identified and explored for kynurenine in the previous subsections, may exist in this larger system. Because of the large size of 3-hydroxykynurenine *O*-β-D-glucoside, the calculations are particularly time-consuming. Therefore, we explored only one additional process that we expect to be of relevance for this glucoside, the 6′-O—H···N2 proton-transfer process (cf. inset in Figure 11 for the numbering of atoms), namely, excited-state deactivation via an electron-driven proton transfer involving the 6′-OH group of the glucose moiety and the ring-amino group of the aminobenzene moiety which is mediated by an excited singlet state of charge-transfer character.

Figure 11 shows the potential-energy profiles of the electronic ground state, the lowest $n\pi^*$ state, and four bright $\pi\pi^*$ states along the proton-transfer reaction path for the 6′-O—H···N2 intramolecularly hydrogen-bonded conformer of 3-hydroxykynurenine *O*-β-D-glucoside. The driving coordinate is the O—H bond length of the 6′-O—H group. It describes the

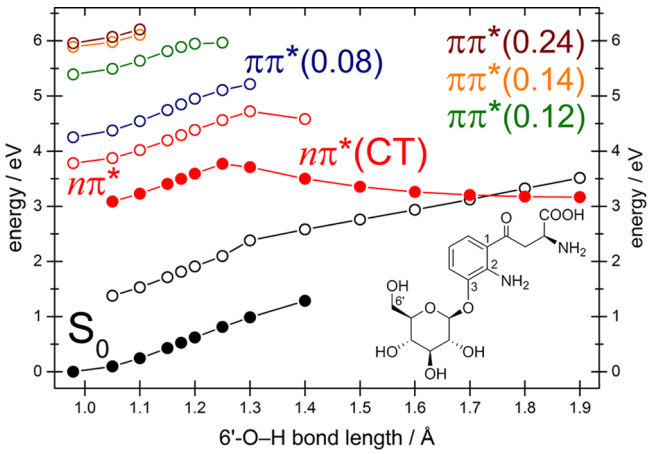

Figure 11. Energy profiles (in eV) of the electronic ground state (S_0), the lowest $n\pi^*$ state, and four optically bright $\pi\pi^*$ states for the 6′-O—H···N2 intramolecularly hydrogen-bonded conformer of 3-hydroxykynurenine *O*-β-D-glucoside. The energy profiles were obtained by a constrained relaxed scan along the O—H bond length of the 6′-OH group in the electronic ground state (full black circles) and in the $n\pi^*$(CT) state (full red circles). The vertical excitation energies of the lowest $n\pi^*$ (empty red circles) and the four $\pi\pi^*$ states (empty blue, green, orange, and purple circles) and the vertical energies of the ground state (empty black circles) are also given. The values of the oscillator strengths at the ground-state equilibrium geometry are given in parentheses. The inset shows the structural formula of 3-hydroxykynurenine *O*-β-D-glucoside with the numbering of atoms. For details, consult the Computational Methods section.

movement of the proton from the 6′-O—H group of the glucose moiety to the N2 nitrogen atom of the aniline moiety of 3-hydroxykynurenine *O*-β-D-glucoside (cf. Figure 11). The full black circles in Figure 11 represent the potential-energy profile of the electronic ground state along the reaction path obtained by a constrained relaxed scan in this state. The vertical excitation energies of the $n\pi^*$ state and of the four bright $\pi\pi^*$ states are given by the empty red, blue, green, orange, and purple circles. The numbers in parentheses specify the oscillator strengths of the excited states at the ground-state equilibrium geometry (structure shown in Figure 12a). All four $\pi\pi^*$ states possess moderately large oscillator strengths. The full red circles represent the potential-energy profile of the lowest $n\pi^*$(CT) state along the reaction path optimized in this state. The energy of the ground state at the same geometries is given by the empty black circles. The lowest $n\pi^*$ state exhibits a clear

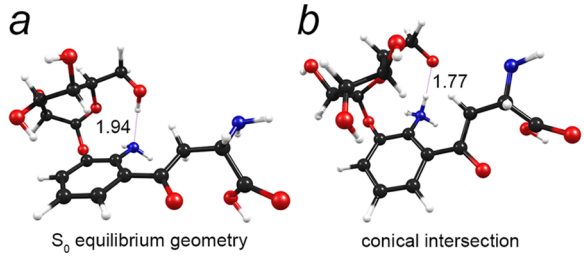

Figure 12. Optimized geometries of 3-hydroxykynurenine *O*-β-D-glucoside: (a) ground-state equilibrium geometry; (b) optimized geometry of the conical intersection for the intramolecular proton-transfer process between the glucose moiety and the aniline moiety. The length of the hydrogen bonds is indicated (in Å). For details, consult the Computational Methods section.

dx.doi.org/10.1021/jp501782v | J. Phys. Chem. B XXXX, XXX, XXX–XXX

charge-transfer character at longer O−H internuclear distances, arising from the translocation of electron density from the 6′-OH group of the glucose moiety to the aniline moiety. This translocation of electron density drives the proton transfer from the 6′-OH group of the glucose moiety to the N2 atom of the aniline moiety. The potential-energy profiles of the charge-transfer state and the electronic ground state intersect at an O−H distance of ∼1.7 Å, which gives rise to a conical intersection (cf. Figure 11). The molecular structure of the conical intersection is shown in Figure 12b. The barrier separating the Franck−Condon region from the S_1/S_0 conical intersection is ∼0.7 eV, but the top of the barrier is still below the vertical excitation energy of the lowest $\pi\pi^*$ state. The barrier for this photochemical deactivation process is thus substantially higher than the proton-transfer barriers in kynurenine. However, it is possible that this barrier is overestimated due to constraints of the relaxed scan (cf. Computational Methods). Although the glucose moiety itself is not a chromophore, internal conversion from the absorbing $\pi\pi^*$ states can lead to the population of the $n\pi^*$ state which involves the lone-pair orbital located at the oxygen atom of the 6′-OH group of the glucose moiety. The charge-transfer character of this $n\pi^*$ state can drive the proton from the glucose moiety to the aniline moiety. The resulting conical intersection between the potential-energy profiles of the $n\pi^*$(CT) state and the electronic ground state may result in internal conversion to the ground state and conversion of electronic energy into vibrational modes of the glucose moiety.

3. DISCUSSION AND CONCLUSIONS

Our exploration of the mechanisms of radiationless excited-state deactivation of photoexcited kynurenines by *ab initio* calculations of photochemical reaction paths and by nonadiabatic trajectory-surface-hopping molecular-dynamics simulations has shown that a number of photochemical mechanisms are accessible in kynurenines for efficiently quenching the energy of absorbed UV photons.

We have shown that the energy profiles of the photochemical reaction paths for the ring-N—H···O═C proton-transfer process in the intramolecularly hydrogen-bonded *cis* conformer of kynurenine and for the tail-N—H···O═C proton-transfer process in the intramolecularly hydrogen-bonded *trans* conformer of kynurenine are essentially barrierless and lead to S_1/S_0 conical intersections. The relevant S_1/S_0 conical intersections are located well below the vertical excitation energy of the lowest bright excited state of $\pi\pi^*$ nature. Both proton-transfer processes are driven by the translocation of electron density from the respective amino group to the keto group in the lowest excited singlet state. Thus, the keto group acts as an electron and proton acceptor of electrons and protons from the amino groups located at the ring and at the terminus of the molecule. The ring-puckering deactivation process of the phenyl ring of kynurenine, on the other hand, has been shown to involve a barrier, like in benzene and aniline.[34−37] The ring-amino-twist mechanism has been shown to be an additional barrierless deactivation process.

The nonadiabatic dynamics simulations of the photochemistry of kynurenine have shown that the *cis* and *trans* conformers of the molecule deactivate on a femtosecond-to-picosecond time scale via proton transfer from an amino group to the keto group. We observed that a large number of trajectories starting in the *trans* conformation underwent *trans* → *cis* isomerization before deactivation via ring-N—H···O═C proton transfer occurred. Only a few of the *trans* conformers did not isomerize and underwent direct deactivation via tail-N—H···O═C or ring-N—H···O═COH proton transfer. Thus, the dynamics simulations suggest that excited-state deactivation via ring-N—H···O═C proton transfer is the dominating and most relevant intramolecular deactivation process in kynurenines. The dynamics simulations have not provided any evidence for the relevance of the ring-puckering mechanism of the phenyl ring for excited-state deactivation of kynurenine but have pointed to the ring-amino-twist mechanism as a possible deactivation process, even though no direct deactivation along this pathway has been observed. Although the TDDFT dynamics simulations are compromising accuracy in favor of lower computational cost, these dynamics simulations nevertheless provide useful insight into the most relevant processes for the excited-state deactivation of kynurenine.

The photochemical reaction path for electron-driven proton transfer between the glucose moiety and the aniline moiety in 3-hydroxykynurenine *O*-*β*-D-glucoside has been shown to involve a barrier. This barrier may be overestimated due to constraints of the relaxed scan which were unavoidable in this case (cf. Computational Methods). Apart from this barrier, the overall picture of this process is very similar to a process that has recently been identified in adenosine: the transfer of a proton from an OH group of the ribose moiety to the N3 heteroatom of the adenine moiety.[39] Additional mechanisms for excited-state deactivation may exist in 3-hydroxykynurenine *O*-*β*-D-glucoside. Glucose, for example, exhibits three types of presumably efficient radiationless deactivation processes via conical intersections: O−H hydrogen-detachment as well as C−O and C−C ring-opening. Aborted photochemical reactions at the S_1/S_0 conical intersections associated with these processes can mediate excited-state deactivation regenerating the reactant.[40] It is a reasonable assumption that 3-hydroxykynurenine *O*-*β*-D-glucoside may also deactivate via the three processes inherent to the glucose moiety. This assumption may rationalize why 3-hydroxykynurenine *O*-*β*-D-glucoside is found in the by far highest concentration of all kynurenines in the ocular lens.

Our combined results from *ab initio* investigations of the photochemical reaction paths for radiationless excited-state deactivation and from nonadiabatic molecular-dynamics simulations show that kynurenines possess a remarkable ability of converting the energy of absorbed UV photons into vibrational energy on a femtosecond-to-picosecond time scale. These findings provide mechanistic evidence of an exceptional UV-filtering capacity of these molecules. We have also shown that the ultrafast excited-state deactivation proceeds primarily via proton-transfer processes, which are mediated by excited singlet states of charge-transfer character and thus provide another example for the significance of electron-driven proton-transfer processes for the UV photostability of biomolecules.[41,42]

To the knowledge of the authors, no experimental data on the photophysics of kynurenine in the gas phase are available. Gas-phase spectroscopy has been performed, however, on 3-hydroxykynurenine using an electrostatic ion-storage ring.[22] Excitation of 3-hydroxykynurenine within the lowest absorption band was found to result in fragmentation to neutral photoproducts and has been interpreted as resulting from efficient internal conversion followed by statistical fragmentation on millisecond time scales.[22] These data are neither conformer-specific nor do they allow a quantitative determi-

dx.doi.org/10.1021/jp501782v | J. Phys. Chem. B XXXX, XXX, XXX−XXX

nation of the rate of internal conversion. More experimental data are available on the photophysics of kynurenine, 3-hydroxykynurenine, and the related chromophore *o*-aminoacetophenone in solution. The latter can be regarded as a simplified model of kynurenine, where the tail of kynurenine is substituted by a methyl group. Vauthey and co-workers investigated the excited-state dynamics of kynurenine in a variety of solvents with femtosecond time-resolved optical spectroscopy.[18] Similar measurements were performed earlier by Yoshihara and co-workers for *o*-aminoacetophenone and some of its derivatives.[43,44] Both kynurenine and *o*-aminoacetophenone exhibit internal conversion as the main channel of excited-state deactivation, but the internal-conversion rate is found to be highly sensitive to the solvent. The shortest fluorescence lifetime ($\tau_f \approx 10$ ps) and the highest quantum yield for internal conversion ($\Phi_{ic} > 0.98$) are observed for *o*-aminoacetophenone in the nonpolar and nonprotic solvents *n*-hexane and cyclohexane[43,44] (no data are available for kynurenine in these solvents). Very short fluorescence lifetimes are also observed for kynurenine in aqueous solution ($\tau_f \approx 30$ ps, $\Phi_{ic} = 0.98$)[18] (no data are available for *o*-aminoacetophenone in water). The rates of internal conversion of both kynurenine and *o*-aminoacetophenone are found to decrease markedly in alcohols and polar aprotic solvents. For example, the internal-conversion rate of kynurenine decreases by more than two orders of magnitude from the solvent water to the solvent dimethyl sulfoxide.[18] Taken together, these experimental findings indicate that kynurenine and the model compound *o*-aminoacetophenone exhibit ultrafast and highly efficient internal conversion in nonpolar solvents (*n*-hexane, cyclohexane) and somewhat reduced, but still ultrafast, excited-state deactivation rates in aqueous solution and simple alcohols, while the radiationless deactivation becomes substantially quenched with increasing polarity of aprotic solvents.[18,43,44]

The present computational studies predict excited-state lifetimes of the order of a few picoseconds for the investigated conformers of isolated kynurenine. Since the internal-conversion process in kynurenine is driven by electron/proton transfer along intramolecular hydrogen bonds, it is not unexpected that these reactions are somewhat slowed down in a strongly protic solvent, since the intramolecular hydrogen bonds have to compete with intermolecular hydrogen bonds to the solvent, which may result in an increase of the proton-transfer barriers of the former. Indeed, the observation of isotope effects in deuterated solvents provides strong evidence that intermolecular hydrogen bonds are involved in the excited-state deactivation of kynurenine and *o*-aminoacetophenone in protic solvents.[18,43] The interplay of intramolecular and intermolecular hydrogen-bond dynamics could be theoretically explored in future studies of the photophysical dynamics in finite-size clusters of kynurenine with water or methanol solvent molecules.

The pronounced effect of the polarity of aprotic solvents on the excited-state deactivation dynamics of kynurenine and *o*-aminoacetophenone seems to not be understood at present and should be explored in future nonadiabatic excited-state quantum-mechanics/molecular-mechanics (QM/MM) simulations. A first step has been undertaken by Benassi and Sherin and by Kessel and co-workers, who have computed the excitation energies of kynurenine and 3-hydroxykynurenine, respectively, in various solvents using a polarized-continuum model and a molecular-dynamics simulation, respectively.[22,24]

Kynurenine is structurally similar to aromatic amino acids and dipeptides. A comparison of the radiationless excited-state deactivation mechanisms in kynurenine with analogous mechanisms found in peptides reveals some noteworthy similarities. In the dipeptide Trp-Gly, for example, the second excited state is the spectroscopically bright $\pi\pi^*$ state located on the indole chromophore. This bright state is connected by a low barrier to a conical intersection with a charge-transfer state. This charge-transfer state drives the transfer of a proton from the acid group at the C-terminus of the molecule to the keto group of the peptide bond.[45] An analogous picture has been found in the tripeptide Trp-Gly-Ala, where the proton transfer occurs between the secondary amine group of the peptide bond and the keto group of the subsequent peptide bond in a so-called γ-turn.[46] While this picture is similar to *trans* kynurenine, in *cis* kynurenine, the S_1 state combines both properties: the spectroscopic "brightness" as well as the photochemical reactivity toward excited-state deactivation via proton transfer. This distinct feature of the S_1 state of the *cis* conformer of kynurenine may be a factor which renders kynurenines exceptionally efficient UV filters.

Kynurenine possesses several excited singlet states of $\pi\pi^*$ character, some of which exhibit a large oscillator strength. The strongly absorbing $\pi\pi^*$ states are located, however, rather high in energy. The cornea absorbs all wavelengths below 300 nm (energies above 4.13 eV). Therefore, the lowest $\pi\pi^*$ state, which is located at ~3.9 eV in the *cis* conformer of kynurenine, at ~4.2 eV in the *trans* conformer of kynurenine, and at ~3.9 eV in 3-hydroxykynurenine *O*-β-D-glucoside, should be the most relevant UV-absorbing state in kynurenines in their natural environment, that is, in an aqueous surrounding in the ocular lens, which is shielded by the partially UV-filtering cornea. Moreover, in an aqueous environment, a moderate red-shift of the excitation energies of the $\pi\pi^*$ states of kynurenines is expected.

The tail of kynurenines, which terminates with a carboxylic group or with an α-amino carboxylic group (i.e., an amino acid moiety, cf. Figure 1), is a residue of the precursor of kynurenines, the amino acid tryptophan. Likely, in the biological system, the function of the tail of kynurenines is to provide good solubility in the aqueous environment. In the zwitterionic form of kynurenines, the tail-N—H···O=C proton-transfer process may not be available for the photoprotective mechanisms, since the amino group at the tail of the molecule may be protonated. Moreover, the deprotonated carboxyl group may be involved in intermolecular hydrogen bonds with surrounding water molecules. Therefore, the ring-N—H···O=COH proton transfer may also be of minor importance in solution. For these reasons, it is possible that the terminal carboxylic group of kynurenines is not of relevance for the photoprotective properties of kynurenines in their natural environment.

Sherin et al. have found that the covalent binding of kynurenine to single amino acids increases the fluorescence quantum yield by a factor of 2, while the covalent binding to a protein increases it by a factor of 7.[19] In the amino-acid and protein adducts, the tail-amino group of kynurenines is substituted by the covalent bond to the amino acid or protein. The experimental observation of Sherin et al. may be rationalized by the steric blocking of the *cis* conformer due to the bulky substituent at the end of the tail, which in turn blocks the ring-N—H···O=C deactivation process and may lead to a significantly longer excited-state lifetime and thus to a larger

dx.doi.org/10.1021/jp501782v | J. Phys. Chem. B XXXX, XXX, XXX–XXX

quantum yield for fluorescence. This indirectly supports our conclusion that the ring-N—H···O=C deactivation process found in *cis* kynurenine is the most relevant deactivation process responsible for the efficient UV-filtering capacity of kynurenines.

While there have been a number of spectroscopic studies performed on kynurenines in various solvents, we hope to stimulate conformer-specific spectroscopic experiments of isolated kynurenines in the gas phase. We have also laid the groundwork for future computational studies of kynurenines in the condensed phase.

4. COMPUTATIONAL METHODS

The second-order Møller−Plesset (MP2) method was used for optimizing ground-state equilibrium geometries and for performing calculations of ground-state potential-energy profiles. The ADC(2) method (algebraic diagrammatic construction of second order)[47−49] was used for excited-state calculations. This methodology offers a description of electronically excited states which is of similar quality as is the MP2 level for the electronic ground state. The potential-energy profiles of the electronic ground state were obtained by constrained optimization at the MP2 level, that is, by fixing the distance between the nitrogen and the hydrogen nuclei (for the processes investigated in kynurenine) and between the oxygen and the hydrogen nuclei (for the process investigated in 3-hydroxykynurenine *O*-*β*-D-glucoside) at a given value and relaxing most of the remaining internal degrees of freedom. It should be noted that, due to the floppiness of the molecule, it was necessary to fix one additional torsion angle in kynurenine (the central C−C−C−C torsion angle along the tail of the molecule) and a number of torsion angles in 3-hydroxykynurenine *O*-*β*-D-glucoside (all torsion angles along the entire tail of the kynurenine moiety) to prevent the tail from changing its conformation from one point of the energy profiles to another. Single-point calculations of excitation energies were performed for the obtained relaxed geometries at the ADC(2) level. The potential-energy profile of the lowest-lying charge-transfer state was obtained by constrained optimization at the ADC(2) level. Single-point energy calculations were performed for the obtained geometries at the MP2 level to obtain the corresponding energies of the ground state. The molecular orbitals shown in Figures 2 and 4 are self-consistent-field orbitals. The reaction paths from the Franck−Condon region to the relevant S_1/S_0 conical intersections shown in Figures 6 and 7 were constructed by linear interpolation in internal coordinates. The energy profiles were obtained by ADC(2) (MP2) single-point energy calculations along the interpolated paths for the excited states (for the ground state). The cc-pVDZ basis set was employed throughout all calculations. These calculations were performed with the Turbomole 6.4 program package.[50]

Minimum-energy conical intersections were optimized using the program package CIOpt developed by Levine, Coe, and Martínez, which allows the optimization of conical intersections without the need of evaluating nonadiabatic couplings,[51] and thus allows the use of electronic-structure methods for which nonadiabatic couplings between adiabatic states are not available, such as the ADC(2) method. The program CIOpt was linked to Turbomole 6.4,[50] and the S_1/S_0 conical intersections were optimized at the mixed ADC(2)/MP2 level.

Nonadiabatic trajectory-surface-hopping molecular-dynamics simulations were performed with time-dependent density functional theory (TDDFT)[33,52−54] employing Tully's fewest-switches surface-hopping procedure.[55] The nonadiabatic-dynamics code is based on localized Gaussian basis sets[31,33,56,57] and was linked to Turbomole 6.4.[50] Newton's equations for nuclear motion were integrated in time steps of 0.5 fs by using the velocity-Verlet algorithm, while the time-dependent Schrödinger equation was integrated using the fourth-order Runge−Kutta method in steps of 0.01 fs. The energy-based decoherence procedure of Granucci and Persico[58] with $\alpha = 0.1E_h$ was used to correct the population of the adiabatic electronic states for the computation of the hopping probabilities. The nonadiabatic-dynamics simulations were performed for the *cis* and *trans* conformers of kynurenine by using the B3LYP exchange-correlation functional and the cc-pVDZ basis set. The functional B3LYP was selected after comparing vertical excitation energies, oscillator strengths, and the physical character of the first few excited states of a number of geometries obtained via a ground-state dynamics simulation computed with the ADC(2) and TDDFT methods employing various DFT functionals. (For a comparison of vertical excitation energies and oscillator strengths for the ground-state equilibrium geometries of *cis* and *trans* kynurenine, see Tables S1 and S2 in the Supporting Information.) To simulate the dynamics of the radiationless excited-state deactivation of kynurenine, we propagated an ensemble of 108 trajectories (58 initial trajectories for the *cis* conformer and 50 initial trajectories for the *trans* conformer) in the subspace of the electronic ground state and four electronically excited states for a total simulation duration of 1.5 ps starting in the S_1 state. The initial conditions were sampled by ground-state dynamics simulations at the RI-PBE/SVP level of theory. These ground-state dynamics simulations were performed at room temperature for a total simulation duration of 15 ps.

■ ASSOCIATED CONTENT

Supporting Information

Optimized geometries of two additional ring-puckered conical intersections. Comparison of vertical excitation energies and oscillator strengths computed at the ADC(2) and TDDFT levels of theory for the *cis* and *trans* conformers of kynurenine. Fourier analysis of the time-dependent potential energy of the ground state between 600 and 975 fs for the trajectory shown in Figure 9. Two additional selected trajectories for the *trans* conformer of kynurenine undergoing *trans* → *cis* isomerization and subsequent excited-state deactivation via ring-N—H···O=C proton transfer and ring-N—H···O=COH proton transfer. Reaction path from the Franck−Condon region to the ring-amino-twisted S_1 equilibrium geometry computed at the TDDFT level of theory. Cartesian coordinates of all optimized ground-state and excited-state equilibrium geometries and all conical intersections. This material is available free of charge via the Internet at http://pubs.acs.org.

■ AUTHOR INFORMATION

Corresponding Author

*E-mail: deniz.tuna@ch.tum.de.

Present Address

⊥Theoretical Chemistry, Max-Planck-Institut für Kohlenforschung, 45470 Mülheim an der Ruhr, Germany.

Notes

The authors declare no competing financial interest.

dx.doi.org/10.1021/jp501782v | J. Phys. Chem. B XXXX, XXX, XXX−XXX

■ ACKNOWLEDGMENTS

D.T. is grateful for a Ph.D. fellowship granted by the International Max Planck Research School of Advanced Photon Science (IMPRS-APS) and for support by the TUM Graduate School. N.D. acknowledges support from the Alexander von Humboldt Foundation and the Unity Through Knowledge Fund. A.L.S. acknowledges a grant by the National Science Center of Poland (Grant No. 2012/04/A/ST2/00100). This work was partially supported by the Cluster of Excellence "Munich-Centre for Advanced Photonics" (MAP).

■ REFERENCES

(1) van Heyningen, R. Fluorescent Glucoside in the Human Lens. *Nature* **1971**, *230*, 393−394.
(2) Wood, A. M.; Truscott, R. J. W. UV Filters in Human Lenses: Tryptophan Catabolism. *Exp. Eye Res.* **1993**, *56*, 317−325.
(3) Wood, A. M.; Truscott, R. J. W. Ultraviolet Filter Compounds in Human Lenses: 3-Hydroxykynurenine Glucoside Formation. *Vision Res.* **1994**, *34*, 1369−1374.
(4) Korlimbinis, A.; Aquilina, J. A.; Truscott, R. J. W. Protein-Bound and Free UV Filters in Cataract Lenses. The Concentration of UV Filters is Much Lower Than in Normal Lenses. *Exp. Eye Res.* **2007**, *85*, 219−225.
(5) Taylor, L. M.; Aquilina, J. A.; Jamie, J. F.; Truscott, R. J. W. UV Filter Instability: Consequences for the Human Lens. *Exp. Eye Res.* **2002**, *75*, 165−175.
(6) Vazquez, S.; Aquilina, J. A.; Jamie, J. F.; Sheil, M. M.; Truscott, R. J. W. Novel Protein Modification by Kynurenine in Human Lenses. *J. Biol. Chem.* **2002**, *277*, 4867−4873.
(7) Korlimbinis, A.; Truscott, R. J. W. Identification of 3-Hydroxykynurenine Bound to Proteins in the Human Lens. A Possible Role in Age-Related Nuclear Cataract. *Biochemistry* **2006**, *45*, 1950−1960.
(8) Roberts, J. E. Ocular Phototoxicity. *J. Photochem. Photobiol., B* **2001**, *64*, 136−143.
(9) Mizdrak, J.; Hains, P. G.; Truscott, R. J. W.; Jamie, J. F.; Davies, M. J. Tryptophan-Derived Ultraviolet Filter Compounds Covalently Bound to Lens Proteins are Photosensitizers of Oxidative Damage. *Free Radicals Biol. Med.* **2008**, *44*, 1108−1119.
(10) Bron, A. J.; Vrensen, G. F. J. M.; Koretz, J.; Maraini, G.; Harding, J. J. The Ageing Lens. *Ophthalmologica* **2000**, *214*, 86−104.
(11) Bova, L. M.; Sweeney, M. H. J.; Jamie, J. F.; Truscott, R. J. W. Major Changes in Human Ocular UV Protection with Age. *Invest. Ophthalmol. Visual Sci.* **2001**, *42*, 200−205.
(12) Kessel, L.; Kalinin, S.; Nagaraj, R. H.; Larsen, M.; Johansson, L. B.-Å. Time-Resolved and Steady-State Fluorescence Spectroscopic Studies of the Human Lens with Comparison to Argpyrimidine, Pentosidine and 3-OH-Kynurenine. *Photochem. Photobiol.* **2002**, *76*, 549−554.
(13) Tsentalovich, Y. P.; Snytnikova, O. A.; Sherin, P. S.; Forbes, M. D. E. Photochemistry of Kynurenine, a Tryptophan Metabolite: Properties of the Triplet State. *J. Phys. Chem. A* **2005**, *109*, 3565−3568.
(14) Tsentalovich, Y. P.; Snytnikova, O. A.; Forbes, M. D. E.; Chernyak, E. I.; Morozov, S. V. Photochemical and Thermal Reactivity of Kynurenine. *Exp. Eye Res.* **2006**, *83*, 1439−1445.
(15) Kopylova, L. V.; Snytnikova, O. A.; Chernyak, E. I.; Morozov, S. V.; Tsentalovich, Y. P. UV Filter Decomposition. A Study of Reactions of 4-(2-Aminophenyl)-4-oxocrotonic Acid with Amino Acids and Antioxidants Present in the Human Lens. *Exp. Eye Res.* **2007**, *85*, 242−249.
(16) Snytnikova, O. A.; Sherin, P. S.; Tsentalovich, Y. P. Biphotonic Ionization of Kynurenine and 3-Hydroxykynurenine. *J. Photochem. Photobiol., A* **2007**, *186*, 364−368.
(17) Sherin, P. S.; Tsentalovich, Y. P.; Snytnikova, O. A.; Sagdeev, R. Z. Photoactivity of Kynurenine-Derived UV Filters. *J. Photochem. Photobiol., B* **2008**, *93*, 127−132.
(18) Sherin, P. S.; Grilj, J.; Tsentalovich, Y. P.; Vauthey, E. Ultrafast Excited-State Dynamics of Kynurenine, a UV Filter of the Human Eye. *J. Phys. Chem. B* **2009**, *113*, 4953−4962.
(19) Sherin, P. S.; Grilj, J.; Kopylova, L. V.; Yanshole, V. V.; Tsentalovich, Y. P.; Vauthey, E. Photophysics and Photochemistry of the UV Filter Kynurenine Covalently Attached to Amino Acids and to a Model Protein. *J. Phys. Chem. B* **2010**, *114*, 11909−11919.
(20) Tsentalovich, Y. P.; Sherin, P. S.; Kopylova, L. V.; Cherepanov, I. V.; Grilj, J.; Vauthey, E. Photochemical Properties of UV Filter Molecules of the Human Eye. *Invest. Ophthalmol. Visual Sci.* **2011**, *10*, 7687−7696.
(21) Zelentsova, E. A.; Sherin, P. S.; Snytnikova, O. A.; Kaptein, R.; Vauthey, E.; Tsentalovich, Y. P. Photochemistry of Aqueous Solutions of Kynurenic Acid and Kynurenine Yellow. *Photochem. Photobiol. Sci.* **2013**, *12*, 546−558.
(22) Kessel, L.; Nielsen, I. B.; Bochenkova, A. V.; Bravaya, K. B.; Andersen, L. H. Gas-Phase Spectroscopy of Protonated 3-OH Kynurenine and Argpyrimidine. Comparison of Experimental Results to Theoretical Modeling. *J. Phys. Chem. A* **2007**, *111*, 10537−10543.
(23) Goswami, N.; Makhal, A.; Pal, S. K. Toward an Alternative Intrinsic Probe for Spectroscopic Characterization of a Protein. *J. Phys. Chem. B* **2010**, *114*, 15236−15243.
(24) Benassi, E.; Sherin, P. S. Theoretical Study of Solvent Influence on the Electronic Absorption and Emission Spectra of Kynurenine. *Int. J. Quantum Chem.* **2011**, *111*, 3799−3804.
(25) Domcke, W., Yarkony, D. R., Köppel, H., Eds. *Conical Intersections: Electronic Structure, Dynamics & Spectroscopy*; World Scientific Publishing: Singapore, 2004.
(26) Olivucci, M., Ed. *Computational Photochemistry*; Elsevier: Amsterdam, The Netherlands, 2005.
(27) Domcke, W., Yarkony, D. R., Köppel, H., Eds. *Conical Intersections: Theory, Computation and Experiment*; World Scientific Publishing: Singapore, 2011.
(28) Barbatti, M. Nonadiabatic Dynamics with Trajectory Surface Hopping Method. *Wiley Interdiscip. Rev.: Comput. Mol. Sci.* **2011**, *1*, 620−633.
(29) Tapavicza, E.; Bellchambers, G. D.; Vincent, J. C.; Furche, F. *Ab Initio* Non-Adiabatic Molecular Dynamics. *Phys. Chem. Chem. Phys.* **2013**, *15*, 18336−18348.
(30) Curchod, B. F. E.; Rothlisberger, U.; Tavernelli, I. Trajectory-Based Nonadiabatic Dynamics with Time-Dependent Density Functional Theory. *ChemPhysChem* **2013**, *14*, 1314−1340.
(31) Mitrić, R.; Werner, U.; Bonačić-Koutecký, V. Nonadiabatic Dynamics and Simulation of Time Resolved Photoelectron Spectra within Time-Dependent Density Functional Theory: Ultrafast Photoswitching in Benzylideneaniline. *J. Chem. Phys.* **2008**, *129*, 164118.
(32) Tapavicza, E.; Meyer, A. M.; Furche, F. Unravelling the Details of Vitamin D Photosynthesis by Non-Adiabatic Molecular Dynamics Simulations. *Phys. Chem. Chem. Phys.* **2011**, *13*, 20986−20998.
(33) Mališ, M.; Loquais, Y.; Gloaguen, E.; Biswal, H. S.; Piuzzi, F.; Tardivel, B.; Brenner, V.; Broquier, M.; Jouvet, C.; Mons, M.; et al. Unraveling the Mechanisms of Nonradiative Deactivation in Model Peptides Following Photoexcitation of a Phenylalanine Residue. *J. Am. Chem. Soc.* **2012**, *134*, 20340−20351.
(34) Palmer, I. J.; Ragazos, I. N.; Bernardi, F.; Olivucci, M.; Robb, M. A. An MC-SCF Study of the S_1 and S_2 Photochemical Reactions of Benzene. *J. Am. Chem. Soc.* **1993**, *115*, 673−682.
(35) Sobolewski, A. L.; Woywod, C.; Domcke, W. *Ab Initio* Investigation of Potential-Energy Surfaces Involved in the Photophysics of Benzene and Pyrazine. *J. Chem. Phys.* **1993**, *98*, 5627−5641.
(36) Li, Q.; Mendive-Tapia, D.; Paterson, M. J.; Migani, A.; Bearpark, M. J.; Robb, M. A.; Blancafort, L. A Global Picture of the S_1/S_0 Conical Intersection Seam of Benzene. *Chem. Phys.* **2010**, *377*, 60−65.
(37) Roberts, G. M.; Williams, C. A.; Yound, J. D.; Ullrich, S.; Paterson, M. J.; Stavros, V. G. Unraveling Ultrafast Dynamics in Photoexcited Aniline. *J. Am. Chem. Soc.* **2012**, *134*, 12578−12589.
(38) Eckert-Maksić, M.; Vazdar, M.; Ruckenbauer, M.; Barbatti, M.; Müller, T.; Lischka, H. Matrix-Controlled Photofragmentation of

Formamide: Dynamics Simulation in Argon by Nonadiabatic QM/MM Method. *Phys. Chem. Chem. Phys.* **2010**, *12*, 12719−12726.
(39) Tuna, D.; Sobolewski, A. L.; Domcke, W. Mechanisms of Ultrafast Excited-State Deactivation in Adenosine. *J. Phys. Chem. A* **2014**, *118*, 122−127.
(40) Tuna, D.; Sobolewski, A. L.; Domcke, W. Electronically Excited States and Photochemical Reaction Mechanisms of β-Glucose. *Phys. Chem. Chem. Phys.* **2014**, *16*, 38−47.
(41) Sobolewski, A. L.; Domcke, W. The Chemical Physics of the Photostability of Life. *Europhys. News* **2006**, *37*, 20−23.
(42) Domcke, W.; Sobolewski, A. L. Peptide Deactivation: Spectroscopy Meets Theory. *Nat. Chem.* **2013**, *5*, 257−258.
(43) Yoshihara, T.; Shimada, H.; Shizuka, H.; Tobita, S. Internal Conversion of *o*-Aminoacetophenone in Solution. *Phys. Chem. Chem. Phys.* **2001**, *3*, 4972−4978.
(44) Shimada, H.; Nakamura, A.; Yoshihara, T.; Tobita, S. Intramolecular and Intermolecular Hydrogen-Bonding Effects on Photophysical Properties of 2′-Aminoacetophenone and its Derivatives in Solution. *Photochem. Photobiol. Sci.* **2005**, *4*, 367−375.
(45) Shemesh, D.; Hättig, C.; Domcke, W. Photophysics of the Trp-Gly Dipeptide: Role of Electron and Proton Transfer Processes for Efficient Excited-State Deactivation. *Chem. Phys. Lett.* **2009**, *482*, 38−43.
(46) Shemesh, D.; Sobolewski, A. L.; Domcke, W. Efficient Excited-State Deactivation of the Gly-Phe-Ala Tripeptide via an Electron-Driven Proton-Transfer Process. *J. Am. Chem. Soc.* **2009**, *131*, 1374−1375.
(47) Schirmer, J. Beyond the Random-Phase Approximation: A New Approximation Scheme for the Polarization Propagator. *Phys. Rev. A* **1982**, *26*, 2395−2416.
(48) Trofimov, A. B.; Schirmer, J. An Efficient Polarization Propagator Approach to Valence Electron Excitation Spectra. *J. Phys. B* **1995**, *28*, 2299−2324.
(49) Wormit, M.; Rehn, D. R.; Harbach, P. H. P.; Wenzel, J.; Krauter, C. M.; Epifanovsky, E.; Dreuw, A. Investigating Excited Electronic States Using the Algebraic Diagrammatic Construction (ADC) Approach of the Polarisation Propagator. *Mol. Phys.* **2014**, *112*, 774−784.
(50) TURBOMOLE V6.4 2012, a development of University of Karlsruhe and Forschungszentrum Karlsruhe GmbH, 1989−2007, TURBOMOLE GmbH, since 2007, available from http://www.turbomole.com.
(51) Levine, B. G.; Coe, J. D.; Martínez, T. J. Optimizing Conical Intersections without Derivative Coupling Vectors: Application to Multistate Multireference Second-Order Perturbation Theory (MS-CASPT2). *J. Phys. Chem. B* **2008**, *112*, 405−413.
(52) Tapavicza, E.; Tavernelli, I.; Rothlisberger, U. Trajectory Surface Hopping within Linear Response Time-Dependent Density-Functional Theory. *Phys. Rev. Lett.* **2007**, *98*, 023001.
(53) Tavernelli, I.; Tapavicza, E.; Rothlisberger, U. Nonadiabatic Coupling Vectors Within Linear Response Time-Dependent Density Functional Theory. *J. Chem. Phys.* **2009**, *130*, 124107.
(54) Tavernelli, I.; Curchod, B. F. E.; Rothlisberger, U. On Nonadiabatic Coupling Vectors in Time-Dependent Density Functional Theory. *J. Chem. Phys.* **2009**, *131*, 196101.
(55) Tully, J. C. Molecular Dynamics with Electronic Transitions. *J. Chem. Phys.* **1990**, *93*, 1061−1071.
(56) Werner, U.; Mitrić, R.; Suzuki, T.; Bonačić-Koutecký, V. Nonadiabatic Dynamics within the Time Dependent Density Functional Theory: Ultrafast Photodynamics in Pyrazine. *Chem. Phys.* **2008**, *349*, 319−324.
(57) Novak, J.; Mališ, M.; Prlj, A.; Ljubić, I.; Kühn, O.; Došlić, N. Photoinduced Dynamics of Formic Acid Monomers and Dimers: The Role of the Double Hydrogen Bond. *J. Phys. Chem. A* **2012**, *116*, 11467−11475.
(58) Granucci, G.; Persico, M. Critical Appraisal of the Fewest Switches Algorithm for Surface Hopping. *J. Chem. Phys.* **2007**, *126*, 134114.